Transparent all-dielectric gradient index waveplates with compact profiles

M. Lorente-Crespo,[1, a)] G.C. Ballesteros,[2] and C. Mateo-Segura[1]
[1)] *Institute of Sensors, Signals and Systems, Heriot-Watt University, EH14 4AS, Edinburgh, UK*
[2)] *Institute of Photonics and Quantum Sciences, SUPA, Heriot-Watt University, EH14 4AS, Edinburgh, UK*

(Dated: 24 August 2016)

Purely dielectric waveplates overcome problems typically associated with metals, e.g. corrosion. However, they are often bulky and/or lossy substantially reducing their applicability. As the operating frequency shifts towards lower frequencies where compactness is a sought after quality, these problems become even more severe. In this letter, we theoretically demonstrate how to combine axially varying gradient index materials with form birefringence to realize nearly transparent and compact dielectric waveplates. The waveplate is subsequently studied considering a discrete distribution of indexes of refraction. Our results indicate that the number of discretization levels required to perform as the continuous gradient index case is small, which would simplify significantly the fabrication process. As an example, a 0.65λ-thick quarterplate with less than 0.1 dB insertion loss at $\sim$34 GHz is designed and compared with full-wave simulations, proving an excellent agreement.

Recent studies focus on the development of all-dielectric waveplates as an alternative to metallo-dielectric structures to alter the polarization state of waves.[1–3] Thanks to their purely dielectric nature, this type of waveplates addresses typical problems associated with metals, e.g. corrosion and low power handling capabilities.[4] All-dielectric waveplates consisting of birefringent crystals with appropriate thickness and orientation have been extensively used in optics.[5,6] Unfortunately, the range of naturally available birefringent materials is very limited at lower frequencies. All-dielectric waveplates exploiting artificial birefringence – form birefringence– have been recently demonstrated in microwaves[7,8] and at terahertz waves.[9–11] Typically, standard form birefringent waveplates consist of a periodic grating of planar dielectric sheets with subwavelength periodicity.[6] The grating is arranged so that its response to electromagnetic waves is anisotropic. In virtue of anisotropy, the phase-shift introduced upon transmission through the waveplate depends on polarization. As a consequence, when a plane wave which can be decomposed in two orthogonally polarized components propagates through the structure, the phase-delay introduced between both components can be tailored to specific values. Thus, varying the thickness and orientation of the waveplate results in a custom rotation of the polarization state at the output. Although promising, form birefringent waveplates are limited in terms of bulkiness (which becomes more severe as the range of operation shifts towards lower frequencies) and/or reflections, i.e. high insertion loss (IL). The trade-off between these two features makes addressing both simultaneously very challenging.

In this letter, we propose to include gradient index (GRIN) media in order to achieve transparency along with compactness. GRIN media have been widely studied in optics and are currently receiving considerable attention mainly in the field of imaging. Luneburg lenses, Eaton lenses or Maxwell's fisheye owe their particular performances to GRIN media.[12] Likewise, GRIN media also find application as antireflection coatings in a myriad of optical systems.[13,14] This type of antireflection coatings minimize reflections by creating a smooth transition between two indexes of refraction so that an electromagnetic wave propagating through such a three layer system, experiences a single continuous medium. Here, we demonstrate how all-dielectric waveplates may benefit from this phenomenon. Potential applications include isolators[15], imaging and monitoring systems,[16,17] and satellite communications.[18]

A typical form birefringent waveplate consisting of a t-thick subwavelength periodic stack of planar dielectric sheets with refractive indexes n_1 and n_2 and widths w_1 and w_2, respectively, is considered in the following, Fig. 1(a). All the media are assumed to be non magnetic ($\mu = 1$). A normal incident plane wave with E-field vector $\boldsymbol{E} = (E_x, E_y)$ is assumed. In the metamaterial regime, i.e. when $w_1 + w_2 \ll \lambda$ being λ the free-space wavelength, such a structure can be described using an effective medium approximation. Hence, its electromagnetic response is equivalent to that of an effective uniaxial anisotropic medium with in-plane refractive index tensor components

$$n_{xx} = \left(\frac{v_1}{n_1^2} + \frac{v_2}{n_2^2}\right)^{-1/2}, \tag{1}$$

$$n_{yy} = \left(v_1 n_1^2 + v_2 n_2^2\right)^{1/2}, \tag{2}$$

where v_1 and v_2 are the volume fractions occupied by each medium and $n_{yy} > n_{xx}$.[6]

No restrictions have been imposed yet to n_1 and n_2 which in the standard case are homogeneous.[7–11] Hereafter, one of the two constituent materials is replaced by a GRIN medium with axial parabolic variation along the

[a)] Electronic mail: ml343@hw.ac.uk

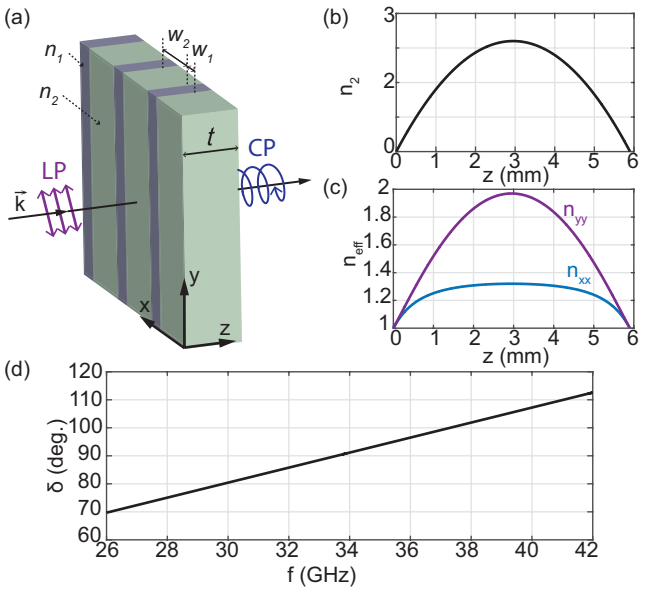

FIG. 1. (color online). (a) Form birefringent waveplate. The dielectric stack extends to infinity in the y-direction and is periodically repeated in x. A normal incident planewave with E-field contained in the xy-plane impinges the structure. (b) Spatial variation of the refractive index of a $t = 5.9$ mm GRIN medium with $n_{\text{out}} = 1$ and $n_{\text{in}} = 2.6$. (c) Effective refractive index values of of a waveplate made of the GRIN medium and air gaps (volume fraction is 50%). (d) Phase-delay between transmitted E-field components.

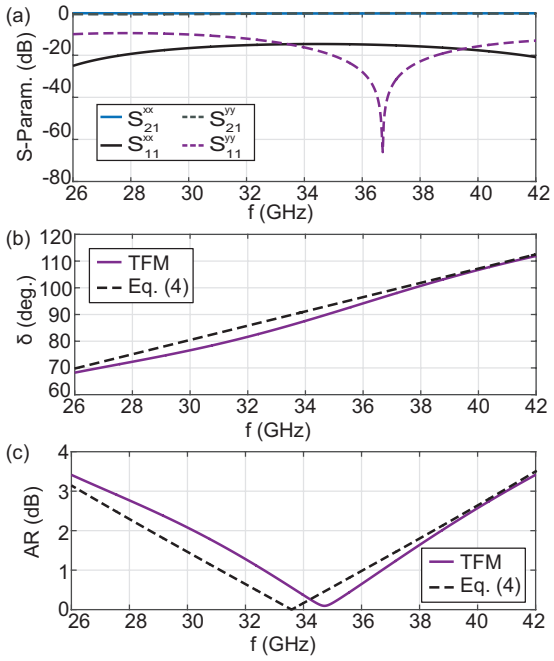

FIG. 2. (color online). (a) S-parameters given by the TFM formalism with N = 100. (b) Phase-delay and (c) AR with (dashed line) and without (solid line) reflections after a LP wave with E-field polarized at 45° from the x-axis propagates through the waveplate.

direction of propagation

$$n_2(z) = \frac{4(n_{\text{out}} - n_{\text{in}})}{L^2}\left(z - \frac{t}{2}\right)^2 + n_{\text{in}}. \qquad (3)$$

In (3), n_{out} and n_{in} represent the refractive indexes at the outer ($z = 0, t$) and inner points ($z = t/2$), respectively. Equation (3) can be used in combination with (1)-(2) to obtain closed-form expressions of the in-plane components of the refractive index tensor of the equivalent medium, $n_{xx}(z)$ and $n_{yy}(z)$. In a reflectionless scenario, the phase-delay introduced upon transmission through the GRIN waveplate can be approximated by the product of the propagation constant and the difference between the light path integral for each field component

$$\delta = \frac{\omega}{c}\int_0^t [n_{xx}(z) - n_{yy}(z)]\, dz. \qquad (4)$$

Without loss of generality, a GRIN medium with $n_{\text{out}} = 1$, $n_{\text{in}} = 2.6$ and $t = 5.9$ mm is considered next. Its index profile as a function of the distance z from the input interface is shown in Fig. 1(b). Planar films made of this material separated by air gaps ($n_1 = 1$) are periodically arranged to build a waveplate, Fig. 1(a). The width of the material with n_1 (air) and the GRIN medium are equal ($w_2 = w_1$), causing 50% volume fractions. The effective refractive indexes of the anisotropic equivalent media given by (1)-(2) and the realized phase-shift according to (4) are shown in Fig. 1(c) and 1(d), respectively. As can be seen, the waveplate introduces 90° phase-delay (quarter wave retardation) between both E-field components at ∼34 GHz.

Despite the gradual variation of the index, small reflections, which have been neglected up to this point, do exist. It has been shown that transmission through a standard form birefringent waveplate is accurately described using a simple transmission line equivalent circuit.[7] Along the same lines, transmission through a GRIN waveplate –or even through a simple GRIN medium– may be understood as a microwave taper. Tapers can be described by transmission lines with gradually varying characteristic impedance and are often modelled using small discretized sections connected in cascade. As the number of sections approaches infinity, the discretized response approaches the continuous case.[19] Propagation through the GRIN-waveplate may be treated analogously as an anisotropic stratified medium. In this sense, the waveplate is discretized in N sections consisting of homogeneous media with equal thickness. Finally, the response of such stratified medium can be approximated using a transfer matrix (TFM) formalism.[6]

A N = 100 discretization of the structure is considered next. The S-parameters obtained using the TFM method are depicted in Fig. 2(a). Reflections are below -9 dB within the considered frequency range, despite the thickness of the waveplate being subwavelength (t

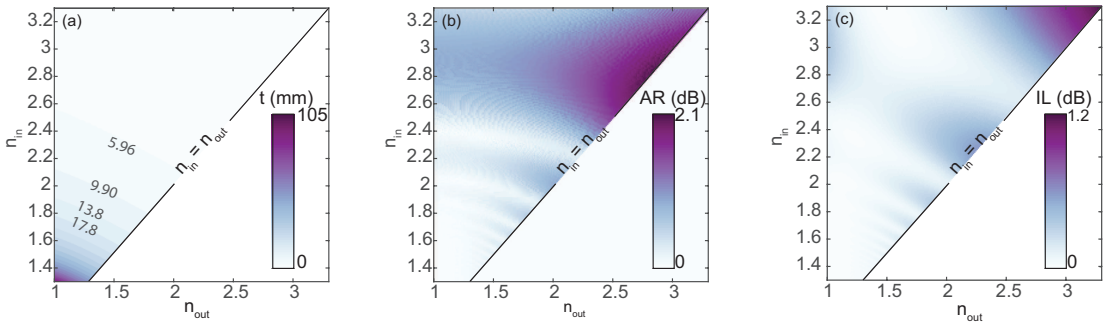

FIG. 3. (color online). (a) Optimum thickness for 90° phase-shift between E_x and E_y. For increased clarity, some values of t have been included. (b) Realized AR and (c) IL as a function of n_{out} and n_{in} for t indicated in (a). (a)-(c) The operating frequency is 34 GHz.

$\sim 0.65\lambda$). As a result, there is almost total transmission for both polarizations. The maximum difference in transmission levels is below 0.6 dB. The estimated phase-delay and axial ratio (AR) given by the TFM method together with that approximated using (4) are shown in Fig. 2(b) and 2(c), respectively. The AR corresponds to that obtained after a linearly polarized (LP) plane wave with E-field polarized at 45° with respect to the x-axis propagates through the waveplate. Results obtained through both procedures are slightly different. When reflections are neglected, as is the case in (4), the phase-difference increases linearly with frequency, Fig. 2(b). On the contrary, the TFM yields a more realistic scenario where reflections are accounted for. These reflections, caused by impedance mismatch not just at the input and output interfaces, as in standard waveplates, but across the whole profile, may result in the formation of a cavity which in turn causes an oscillatory phase-difference. Since in this case reflections are small, the cavity formed is very weak and so is the amplitude of the oscillations in Fig. 2(b)-2(c). Despite also present in the transmission parameters, oscillations are hard to appreciate in Fig. 2(a). Since the transmitted power for both polarization components is very similar, $\delta = 90^\circ$ produces nearly perfect linear to circular polarization conversion (AR $\sim$ 0 dB), as suggested by Fig. 2(b)-2(c), with 40% 3dB AR fractional bandwidth.

The flexibility in the choice of GRIN medium is investigated in Fig. 3 where results for different combinations of n_{out} and n_{in} are shown. The study is limited to $n_{\text{in}} \geq n_{\text{out}}$. Fig. 3(a) shows the optimum thickness of the waveplate for 90° phase-delay at 34 GHz computed from (4). The optimum values where obtained using the simplex optimization algorithm. A singularity occurs when the effective indexes match the index of the background, i.e. when $n_{\text{out}} = n_{\text{in}} = 1$, for which $t \to \infty$ (not shown). For fixed n_{out}, the required thickness for quarter wave retardation rapidly decreases with increasing n_{in} (higher index contrast). If n_{in} is fixed instead, a higher value of n_{out} results as well in a higher contrast, yielding more compact devices. However, the thickness decrease is slower when n_{out} is increased instead of n_{in}.

Fig. 3(b) and 3(c) show the AR and IL at 34 GHz, respectively, calculated using the TFM when the incident wave is LP at 45° and the waveplate has the thickness shown in Fig. 3(a). Note that the achieved AR does not vanish for all the cases under consideration, the reason for this is twofold. On the one hand, the phase-delay introduced when the thickness is derived from (4) differs up to 8° from the TFM model. The differences between these two methods were already shown in Fig. 2(b). However, optimization is greatly simplified by using (4) and the values estimated using this procedure may provide a good starting point for a subsequent optimization using the TFM or a full-wave electromagnetic solver, in case higher accuracy is required. On the other hand, for a pure CP wave (i.e. AR = 0 dB) the magnitude of each transmitted E-field component shall be equal. Reflections due to the inhomogeneous index distribution cause oscillations in the transmission parameter, and thus in the transmitted power, which in turn deteriorates the polarisation purity. Since the condition $n_{xx} \neq n_{yy}$ shall be satisfied to provide birefringence, coupling of electromagnetic waves to the cavity depends on polarization. As a result, the power transmitted for each polarization may differ giving non-zero values of the AR. Remarkably, it remains below 1 dB for most of the indexes combinations, being the maximum AR = 2.1 dB without any further optimization. Lastly, the IL is shown in Fig. 3(c). Note that, for lossless dielectrics as those considered here, IL can be merely attributed to reflections. The low IL reported (IL $<$ 1.2 dB) together with the small thickness and low AR prove that GRIN waveplates are an excellent alternative to typical form birefringent waveplates,[7] since they enable reducing dimensions and IL simultaneously without compromising performance.

Several techniques are available for fabricating GRIN media. Drilling a gradient of subwavelength holes on an ordinary dielectric material[20] is among the simpler alternatives. The same effect may be achieved using 3D

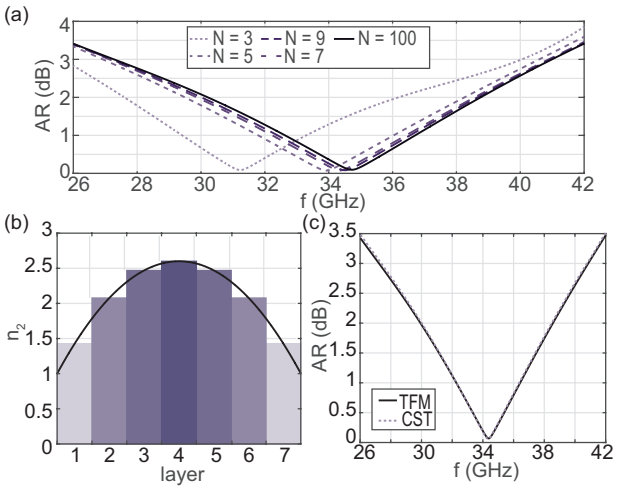

FIG. 4. (color online). (a) AR as a function of the number of discretization steps. (b) Spatial variation of the continuous (black curve) and N = 7 discretized index profile. (c) AR calculated using the TFM formalism and through full-wave simulations with $w_1 = w_2 = 0.5$ mm and $\tan(\delta) = 0.0072$.

printing technology.[21] A different approach consists of discretizing the index profile and replacing the GRIN medium by a collection of homogeneous dielectrics. The required indexes may be provided in practice by composite materials, e.g. resins loaded with ceramic powders.[22] In preparation for a practical realization, the discretization is studied in Fig. 4. Fig. 4(a) shows the AR obtained from the TFM method with different number of discretization steps. As can be seen in the figure, results rapidly converge for increasing N. Note that results obtained with as little as N = 7 are nearly identical to those obtained with N = 100 ($< 1.5\%$ and 0.02 dB difference in frequency and minimum AR) which suggests that the fabrication of the proposed GRIN waveplate is feasible. Similarly, our studies showed that matching and IL do not exhibit significant deviations for $N > 7$. The N = 7 case is further investigated in Fig. 4(b)-(c). The index of refraction of the discretized GRIN material is shown in Fig. 4(b). For the sake of comparison, the ideal continuous profile has been included. The AR for lossy dielectrics is depicted in Fig. 4(c). In particular, we used $\tan(\delta) = 0.0072$ for modelling typical losses of composite materials.[22] As shown, the AR calculated using the TFM and that obtained via full-wave simulations performed using CST Microwave Studio are in excellent agreement (deviations < 0.03 dB). Likewise, no significant differences were found in the reflection parameters and IL ($< 1\%$ and < 0.01 dB in frequency and magnitude, respectively), validating the accuracy of the TFM method employed throughout this letter. CST simulations show up to 30° angular stability, < -10 dB maximum reflectivity and < 0.33 dB IL.

In conclusion, we have shown how GRIN materials may be employed to realize waveplates. The proposed GRIN waveplates outperform typical form birefringent waveplates as they can exhibit low IL and compact profiles simultaneously which are sought-after features, for instance, in satellite applications –∼70% thickness reduction compared to our previous work.[7] Comparison of the spectral response of GRIN waveplates calculated using a TFM formalism is in excellent agreement with full-wave simulations. Furthermore, we showed how an approximate analytical solution (neglecting reflections) may be used to rapidly evaluate its performance and become the base of a second optimization using a more accurate model, e.g. the TFM method or full-wave simulations. A discretized GRIN waveplate has been proposed to ease the fabrication process. Our results suggest that 7 levels of discretization suffice to implement the GRIN waveplate without degrading its performance, even when typical dielectric losses[22] were considered.

ACKNOWLEDGMENTS

The authors thank the funding support from EPSRC (EP/L015110/1) and FP7 project DORADA (IAPP-2013-610691).

[1] C. W. Haggans, L. Li, T. Fujita, and R. K. Kostuk, J. of Mod. Opt. **40**, 675 (1993).
[2] M. Navarro-Cia, P. Rodriguez-Ulibarri, V. Torres, and M. Beruete, IEEE Photon. Technol. Lett **24**, 945 (2012).
[3] E. Doumanis, G. Goussetis, J. Gomez-Tornero, R. Cahill, and V. Fusco, IEEE Trans. Antennas Propag **60**, 212 (2012).
[4] A. Jain, P. Tassin, T. Koschny, and C. M. Soukoulis, Phys. Rev. Lett. **112**, 117403 (2014).
[5] E. Hecht, *Optics*, 2nd ed. (Addison-Wesley, 1987).
[6] M. Born and E. Wolf, *Principles of Optics: Electromagnetic theory of propagation interference and diffraction of light*, 6th ed. (Cambridge University Press, 1993).
[7] M. Lorente-Crespo, G. C. Ballesteros, G. Goussetis, and C. Mateo-Segura, in press (2016).
[8] J. Zhao, L. Zhang, J. Li, Y. Feng, A. Dyke, S. Haq, and Y. Hao, Sci. Rep. **5** (2015).
[9] M. Scheller, C. Jördens, and M. Koch, Opt. Express **18**, 10137 (2010).
[10] B. Scherger, M. Scheller, N. Vieweg, S. T. Cundiff, and M. Koch, Opt. Express **19**, 24884 (2011).
[11] O. Graydon, Nat. Photon. **6**, 75 (2012).
[12] E. W. Marchand, *Gradient Index Optics*, United Kingdom ed. (Academic Press, 1978).
[13] W. H. Southwell, Opt. Lett. **8**, 584 (1983).
[14] D. Chen, Sol. Energ. Mat. Sol. Cells **68**, 313 (2001).
[15] S. Hollung, W. Shiroma, M. Markovic, and Z. Popovic, IEEE Microw. Guided Wave Lett. **6**, 205 (1996).
[16] C. Dietlein, A. Luukanen, Z. Popovic, and E. Grossman, IEEE Trans. Antennas and Propag. **55**, 1804 (2007).
[17] M. Euler, V. Fusco, R. Cahill, and R. Dickie, IEEE Trans. Antennas Propag **58**, 2457 (2010).
[18] N. Fonseca and C. Mangenot, IEEE Trans. Antennas Propag. **64**, 640 (2015).
[19] D. M. Pozar, *Microwave Engineering* (John Wiley & Sons, 2005).
[20] Z. L. Mei, J. Bai, and T. J. Cui, J. Phys. D: Appl. Phys. **43**, 055404 (2010).
[21] T. A. Campbell and O. S. Ivanova, Nano Today **8**, 119 (2013).
[22] C. Mateo-Segura, A. Dyke, H. Dyke, S. Haq, and Y. Hao, IEEE Trans. Antennas Propag. **62**, 1945 (2014).